Preferentially orientated precipitation in MnTiO₃ single crystals

H. TAKEI
The Research Institute for Iron, Steel and Other Metals, Tohoku University, Sendai 980, Japan

Preferentially orientated precipitation of α-TiO_2 (rutile) needles in single crystals of $MnTiO_3$ grown by a floating-zone method under a controlled atmosphere of oxygen fugacity was studied. Optical microscopy and X-ray analysis revealed that the orientation relation between the α-TiO_2 precipitates and the $MnTiO_3$ matrix is: $\{0\,0\,0\,1\}MnTiO_3\,/\!/$ $\{1\,1\,1\}\alpha$-TiO_2 and $\langle 1\,1\,\bar{2}\,0\rangle MnTiO_3\,/\!/\,\langle 1\,1\,0\rangle\alpha$-$TiO_2$. The precipitation phenomenon was explained by introducing a nucleation and growth mechanism which was experimentally supported by heat treating experiments.

1. Introduction
The study of preferentially orientated precipitation of crystals is of great importance because such phases sometimes give rise to significant changes in the mechanical properties of the original matrix [1–5]. Among oxides containing Mn ions, precipitations thus orientated have been reported by many authors [6–9]. Delavignette and Amelinckx [6] have observed an orientated precipitation of Mn_3O_4 in single crystals of MnO, where excess oxygen in MnO caused the precipitation of Mn_3O_4. Other examples of such phenomena have been found on Mn-ferrite [7], Mn·Fe-spinel [8] and $Mn_{1-x}O$ [9].

In a previous report, the present author described how an orientated needle-like precipitation which was supposed to be of titanium oxide was found in the peripheral region of single crystals of $FeTiO_3$ grown by the floating-zone method [10]. The formation of needles was explained by supersaturated Ti^{4+} ions in the $FeTiO_3$ matrix which were introduced by oxidation of iron ions.

The purpose of the present study was to obtain information on the precipitation of titanium oxide from an ilmenite matrix, and to clarify the orientation relationship between precipitates and matrix. Single-crystal specimens of $MnTiO_3$ were chosen as a matrix substance for the following reasons: (1) the same kind of precipitation as that found in $FeTiO_3$ was found in $MnTiO_3$, (2) the needle was much longer and denser, and (3) clearer

patterns were easily observed under a polarized transmitted light.

2. Experimental procedure
2.1. Crystal growth of MnTiO₃
Single crystals of $MnTiO_3$ were grown by the floating-zone method under a controlled atmosphere of oxygen fugacity using a lamp-image type furnace, which has been described elsewhere [10, 11]. As has already been reported [12], $MnTiO_3$ melts incongruently. Thus, the travelling-solvent technique was applied to this material. Details of the technique are the same as those presented by Shindo *et al.* [13].

Typical growth conditions are as follows: the growth axis was seeded mainly in the $\langle 1\,0\,\bar{1}\,0\rangle$ and subsidiarily in the $\langle 1\,1\,\bar{2}\,0\rangle$, growth rates ranged from 1 to $3\,\mathrm{mm\,h^{-1}}$, the seed and the nutrient rotation rates were both 30 rpm in opposite directions, and the mixed gas flow rates were fixed at the values of $500\,\mathrm{ml\,min^{-1}}$ for CO_2, $5\,\mathrm{ml\,min^{-1}}$ for H_2 and $800\,\mathrm{ml\,min^{-1}}$ for N_2, respectively. The as-grown boules, as shown in Fig. 1, were typically dark brown with dimensions 7 mm diameter and 70 mm long.

2.2. Analyses of MnTiO₃ crystal and precipitates
The composition of the as-grown boules was determined chemically by an oxidation-reduction titration. The results are: Mn, 35.1 wt%, Ti, 32.0
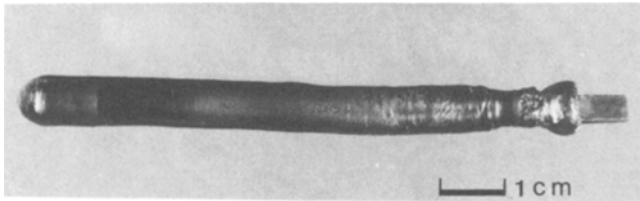
  © *1981 Chapman and Hall Ltd.*

wt%, corresponding to the chemical formula $Mn_{0.96}Ti_{1.02}O_3$. The unit cell parameters at room temperature were $a_0 = 5.138$ Å and $c_0 = 14.279$ Å for hexagonal symmetry. These values are very close to those previously reported [14]. The antiferromagnetic Néel point was estimated to be at 64 K and the maximum magnetic susceptibility along the c-axis was 7.9×10^{-5} emu g^{-1} [15, 16]. A distinct $\{0\,0\,0\,1\}$ cleavage was observed.

Cut and polished sections of the crystal were examined under a transmission microscope as they were sufficiently transparent and brownish yellow in the transmitted light of a tungsten lamp. It was found that acicular, preferentially orientated precipitates existed in peripheral regions within about 500 μm of the boule surfaces (see Fig. 2). The patterns are quite similar to those observed in $FeTiO_3$ crystals [10]. Imperfections such as small-angle grain boundaries, gas bubbles, microcracks,

or further inclusions, other than the acicular precipitates were not found. X-ray precession photography and scanning electron microscopy electron-probe microanalysis (SEM-EPMA) were performed using a Rigaku 1531 camera and an Hitachi–Horiba EMAX-8000 apparatus, respectively. Table I is a summary of the properties.

2.3. Heat treatment in CO_2 atmosphere

Plate-like specimens about 1 mm thick and 4 mm × 3 mm in area, were cut parallel to the $\{0\,0\,0\,1\}$ plane from an unprecipitated part of the as-grown boule. They were carefully polished by metallurgical techniques to mirror surfaces.

Heat treatment was conducted in a 0.3 ml Pt crucible using a Pt–Rh resistance furnace mounted in an air-tight vessel. The atmosphere was CO_2 gas with a flow rate of 300 ml min^{-1}. Eight kinds of heating programmes were provided, as illustrated in Fig. 3. All specimens were heated at 1200° C for 1 h and then cooled according to the programme shown in Fig. 3. After treatment, the specimens were examined under a transmission/reflection microscope and analysed by SEM-EPMA or by the X-ray precession technique.

3. Results and discussion
3.1. Precipitation in the as-grown boule

Optical examination revealed that the acicular precipitates observed in peripheral regions lay in the $\{0\,0\,0\,1\}$ plane.

As already shown in Fig. 2, the length of the needles ranged from about 200 μm to about 5 μm. The density of precipitates varied simultaneously with the length. The longer needles tended to be located near the surface where a low density of precipitation was observed and vice versa.

A sharp delineation between precipitated and unprecipitated regions could not be achieved. However, a rough boundary was estimated by examining the $\{0\,0\,0\,1\}$ sections under a polarized light since the precipitated portion was highly strained with the inclusions. From SEM observation, the diameter of the needles was found to
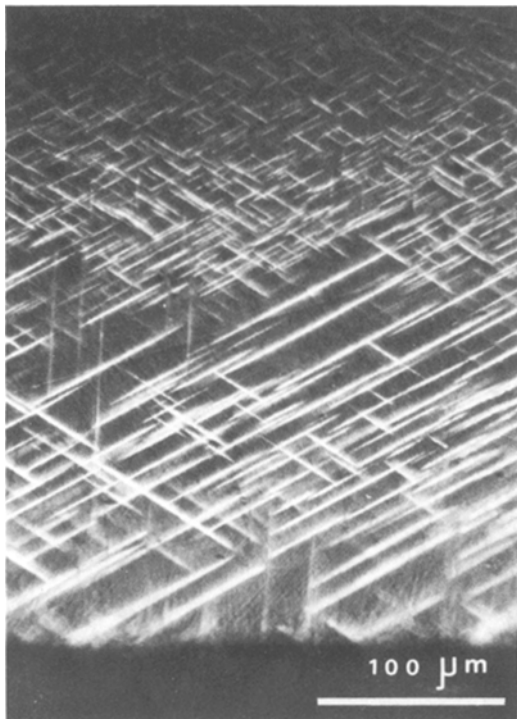

Figure 2 Preferentially orientated precipitates in the as-grown $MnTiO_3$ crystals.

TABLE I Properties of $MnTiO_3$ crystals

Colour:	brownish yellow (thin section)
Lattice constants:	$a_0 = 5.138$ Å ⎫ hexagonal
	$c_0 = 14.279$ Å ⎭ symmetry
Average chemical formulae:	$Mn_{0.96}Ti_{1.02}O_3$
Melting point:	$1360°$ C, incongruent
Cleavage:	(0 0 0 1) distinct
Antiferromagnetic Néel point:	about 64 K
Maximum magnetic susceptibility:	7.9×10^{-5} emu g^{-1} (along c-axis)

remain in the range 0.1 to 1.0 μm. The fact that the precipitation is only observed in the peripheral regions is attributable to oxidation of manganese ions by the atmosphere during cooling. Details of the oxidation will be discussed in a later section.

The results of the EPMA on the $\{0\,0\,0\,1\}$ plane are shown in Fig. 4, where the specimen surface was scanned with an electron beam along the growth axis $\langle 1\,0\,\bar{1}\,0 \rangle$. A sharp increase in the Ti signal and a respective decrease in that of Mn were observed around the needle. Although the precipitates were too shallow to allow a reliable quantitative analysis, the data imply that the needles are of titanium oxide.

Single-crystal X-ray photography of the precipitated region was carried out by the precession technique using MoKα radiation. A piece of the polished specimen containing relatively longer needles, typically 0.5 mm × 0.5 mm in area and 0.2 mm thick, was mounted on the camera with the X-ray beam perpendicular to the reciprocal plane $\{0\,0\,0\,1\}^*$ and $\{1\,0\,\bar{1}\,0\}^*$ of $MnTiO_3$. Fig. 5 is a result of the $\{0\,0\,0\,1\}^*$ photograph, where 24 extra spots which cannot be explained by the diffraction with the $MnTiO_3$ lattice are observed. Calculation of the interspacings of the extra spots indicated that there existed only two kinds of diffraction which gave two d-values, 2.49 Å and 1.35 Å. The angles between the traces of the spots are shown in Fig. 6. From these data, it was concluded that the spots corresponded to the diffraction 1 0 1 and 1 1 2, of α-TiO_2 (rutile).

The orientation relationship between the precipitated rutile and the $MnTiO_3$ matrix is illustrated in Fig. 6, where the left, large circle schematically represents the reciprocal lattice of α-TiO_2 on the $\{0\,0\,0\,1\}^*$ plane of $MnTiO_3$. In this figure, the diffraction spots of α-TiO_2 are only represented by black dots. The small circle, on the right-hand side of the figure, schematically
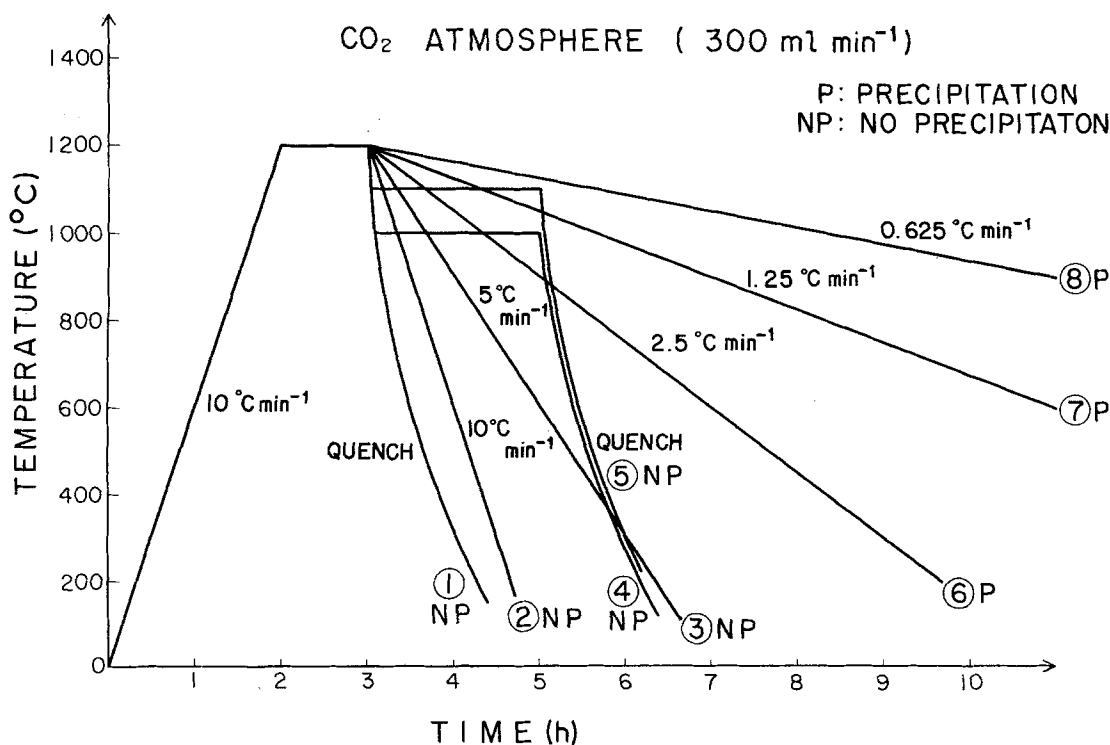

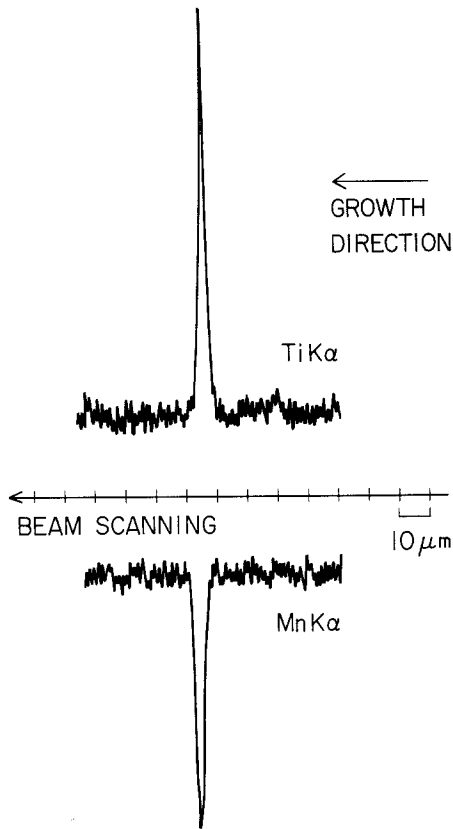Figure 3 Heating and cooling treatments, Programmes 1 to 8, for the $MnTiO_3$ crystals in CO_2.

GROWTH DIRECTION

TiKα

BEAM SCANNING

$10\,\mu m$

MnKα

Figure 4 EPMA pattern on the (0 0 0 1) as-grown surface of the MnTiO₃ crystal.

represents the preferential orientation of the α-TiO₂ needles in real space, whose relations are: $\{1\,1\,1\}\alpha\text{-TiO}_2 /\!/ \{0\,0\,0\,1\} \text{MnTiO}_3$, and $\langle 1\,0\,1 \rangle \alpha\text{-TiO}_2 /\!/$ nearly $\langle 1\,1\,\bar{2}\,0 \rangle \text{MnTiO}_3$. Six pairs of symmetrical dots ($1\,1\,2$ and $1'1'2'$, for example) can be

Figure 5 Precession photograph of precipitated MnTiO₃ crystal.

recognized in this figure. This means that α-TiO₂ precipitates in six different orientations. The difference in orientation from one to another is about 8°.

Formation of the paired orientation in the rutile precipitation can presumably be understood by considering the atomic configuration of MnTiO₃ and α-TiO₂. As is shown in Fig. 7, there are two possible alignments for fitting Ti⁴⁺ions in the (1 1 1) rutile lattice to the (0 0 0 1) oxygen framework of MnTiO₃, where the [1 1 $\bar{2}$ 0] direction of MnTiO₃ is parallel to the [1 $\bar{1}$ 0] of α-TiO₂. This

ELONGATION AXIS OF NEEDLE

a_{MT}^*

$a_{MT}'^*$

36.2°

8°

$1'1'2$ · 112

101 · $1'0'1'$

$10\bar{1}$

$1\bar{1}\bar{2}$

RECIPROCAL LATTICE (0001)* OF MnTiO₃
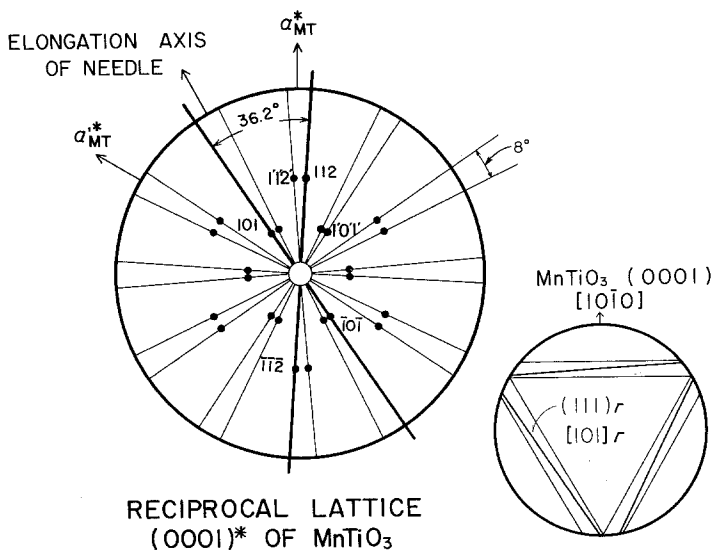
MnTiO₃ (0001)
[10$\bar{1}$0]

(111)r
[101]r

Figure 6 The orientation relationship between the precipitated rutile and the MnTiO₃ matrix. The large circle (left) is an illustration of the reciprocal lattice and the small one (right) shows a schematic drawing of rutile and MnTiO₃ in real space.
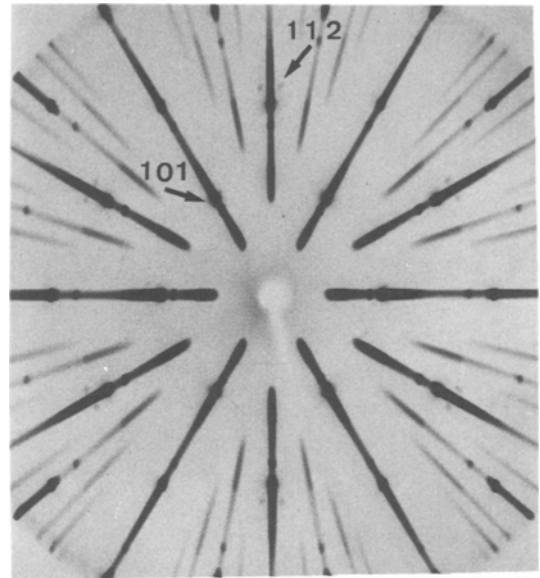
1313

$$Mn\overline{Ti}O_3 \; (000I) \; /\!/ \; TiO_2 \; (111)$$
$$Mn\overline{Ti}O_3 \; [11\overline{2}0] /\!/ \; TiO_2 \; [1\overline{1}0]$$

○ : O^{2-} AT (000I) OF $MnTiO_3$

● : Ti^{4+} AT (111) OF $\alpha-TiO_2$

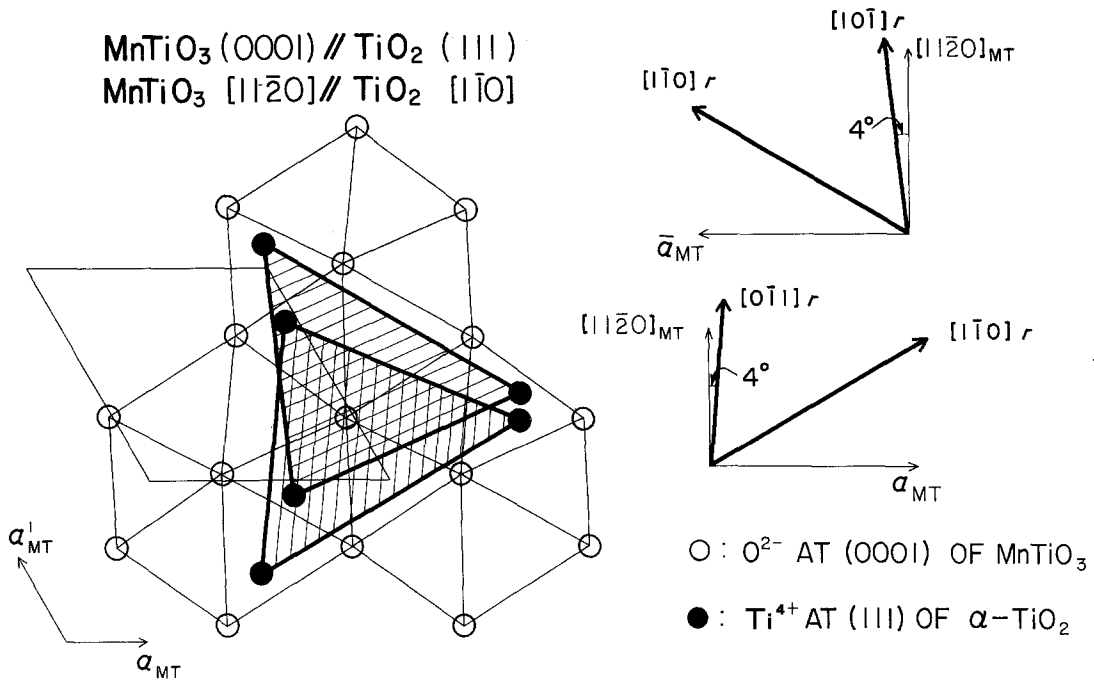*Figure 7* Attachment of Ti^{4+} ions in the (1 1 1) rutile lattice to the (0 0 0 1) $MnTiO_3$ oxygen framework.

leads to the result that the rutile ⟨1 0 1⟩ direction makes an angle of 4° to the ⟨1 1 $\overline{2}$ 0⟩ of $MnTiO_3$. Thus, the orientation relationship between the two crystals can be described as:

and
$$\{0\,0\,0\,1\}MnTiO_3 /\!/ \{1\,1\,1\}\alpha\text{-}TiO_2$$
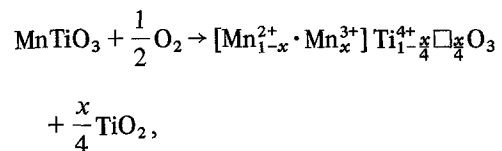$$\langle 1\,1\,\overline{2}\,0\rangle MnTiO_3 /\!/ \langle 1\,1\,0\rangle\alpha\text{-}TiO_2.$$

3.2. Precipitation by heat treatment

Heat treatment was performed in a CO_2 gas flow under heating and cooling programmes, as shown in Fig. 3. As is indicated in the Mn–O phase diagram [17], the equilibrium partial pressure of oxygen for MnO is below 10^{-5} atm, and that for CO_2 gas is about 10^{-3} atm, at 1200° C. Thus, the CO_2 atmosphere probably plays a considerable role in oxidizing Mn^{2+} ions to Mn^{3+} for $MnTiO_3$ at 1200° C. Optical examination revealed that the quenched or rapidly cooled specimens, which were treated according to Programmes 1 to 5 in Fig. 3, did not exhibit a detectable change in surface appearance except for a remarkable change in colour from brownish yellow to dark brown, and consequently a decrease in transmittance of visible light. Precipitation took place when the specimen was heated to 1200° C for 1 h and then cooled slowly according to Programmes 6 to 8.

Fig. 8 shows a typical micrograph of the as-precipitated surface of the $MnTiO_3$ crystals, where the precipitates appeared as preferentially oriented needles like those observed in the peripheral region of the as-grown $MnTiO_3$ boules. The precipitated materials and the crystallographic orientation relation to the matrix was measured under the microscope and by the X-ray precession method. The results showed that the needles were also of $\alpha\text{-}TiO_2$ and were orientated in the same relation as found in the as-grown boules.

The precipitation phenomena can be explained by the occurrence of an excess amount of TiO_2 during heat treatment in CO_2. The excess TiO_2 molecules are thought to be produced by the following oxidation reaction:

$$MnTiO_3 + \frac{1}{2}O_2 \rightarrow [Mn^{2+}_{1-x} \cdot Mn^{3+}_x] \, Ti^{4+}_{1-\frac{x}{4}} \square_{\frac{x}{4}} O_3$$

$$+ \frac{x}{4} TiO_2,$$

where $\square$ represents the vacant site of Ti. This reaction is essentially the same kind as that previously reported [10]. The occurrence of Mn^{3+} in the matrix should bring about significant changes in colour, as described above.

There exists a sharp contrast between Figs 2 and 8. That is, homogeneously long needles with a
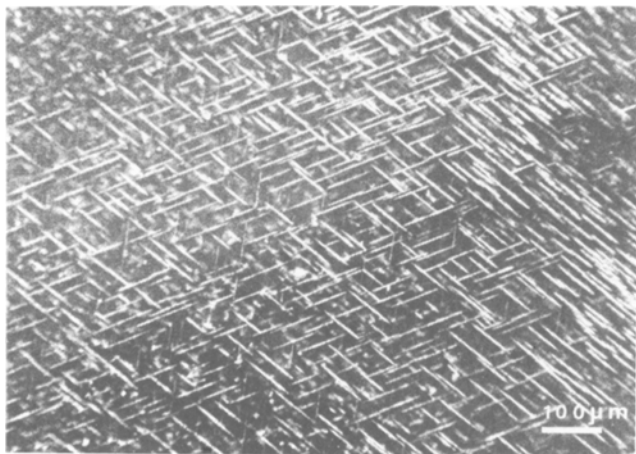
1314

higher density were observed on the heat-treated crystal surfaces. Bratton [3] has reported in a study of high-temperature ageing in the star sapphire that the lengths of the needle-like precipitates were functions of temperature and ageing time. Busovne *et al.* [5] indicated that dislocations acted as nucleation sites for solid-state growth of α-TiO_2 needles in Ti^{4+}-doped sapphire [5]. In the present study, two possible explanations were considered:

(a) temperature and/or time of heat treatment would be adequate to cause growth of the needles;

(b) there would be a much higher density of nucleation sites on the polished surfaces than in the peripheral region of the boules.

However, the present data are insufficient to support these hypotheses and further information on the growth kinetics of needle crystals is needed to explain the precipitation mechanism.

As stated above, it was postulated that an excess number of TiO_2 molecules or Ti^{4+} ions originated by heat treatment in CO_2 would diffuse through the matrix and would precipitate on the nucleation sites. It was also postulated that when the specimens were cooled slowly (Fig. 3, Programmes 6 to 8), the excess Ti^{4+} or TiO_2 could migrate and arrive at a nucleation site. On the other hand, it was thought that the rapid cooling (Fig. 3, Programmes 1 to 3) would provide insufficient time for migration, and that the excess species would stay in the matrix in the form of ions, molecules or fine aggregates.

However, no precipitation was observed when the treatments were conducted according to Programmes 4 or 5 in Fig. 3, where the specimens were heated isothermally at 1100 or 1000°C for 2 h after being pre-heated at 1200°C for 1 h, and then quenched to room temperature. This fact implies that the diffusion rate of TiO_2 or Ti^{4+} in the $MnTiO_3$ matrix may be significantly reduced below 1100°C, and that the cooling rate between 1200 and 1100°C may be the most important factor in needle growth.

4. Conclusions

Preferentially orientated precipitations were examined on both as-grown and heat-treated specimens of $MnTiO_3$ single crystals. The precipitates were of α-TiO_2 needles with orientation relations: $\{0\,0\,0\,1\}MnTiO_3 \,/\!/\, \{1\,1\,1\}\alpha$-$TiO_2$ and $\langle 1\,1\,\bar{2}\,0\rangle MnTiO_3 \,/\!/\, \langle 1\,\bar{1}\,0\rangle\alpha$-$TiO_2$. The experiment indicates that the excess amount of TiO_2 originated from the $MnTiO_3$ matrix by oxidation of Mn^{2+} to Mn^{3+} under a CO_2 atmosphere. The phenomenon involves the nucleation and a growth mechanism in the solid-state during cooling.

Acknowledgements

References

1. J. R. RASMUSSEN, G. B. STRINGFELLOW, I. B. CUTLER and S. D. BROWN, *J. Amer. Ceram. Soc.* 48 (1965) 146.

2. S. E. HSU, W. KOBES and M. E. FINE, *ibid.* **50** (1967) 149.
3. R. J. BRATTON, *J. Appl. Phys.* **42** (1971) 211.
4. E. W. KRUSE III, and M. E. FINE, *J. Amer. Ceram. Soc.* **55** (1972) 32.
5. B. J. BUSOVNE, Jr, D. M. KOTCHIK and R. E. TRESSLER, *Phil. Mag.* **39** (1979) 265.
6. P. DELAVIGNETTE and S. AMELINCKX, *Mat. Res. Bull.* **5** (1970) 1009.
7. J. T. GRUIJTERS and G. D. RIEK, *J. Crystal Growth* **10** (1971) 207.
8. E. H. L. J. DEKKER and G. D. RIEK, *ibid.* **23** (1974) 143.
9. H. R. HARRISON, R. ARAGÓN and C. J. SANDBERG, *Mat. Res. Bull.* **15** (1980) 571.
10. H. TAKEI and K. KITAMURA, *J. Crystal Growth* **44** (1978) 629.
11. H. TAKEI, *ibid.* **43** (1978) 463.
12. J. GREIVE and J. WHITE, *J. Roy. Tech. Coll. (Glasgow)* **4** (1940) 661.
13. I. SHINDO, N. KIMIZUKA and S. KIMURA, *Mat. Res. Bull.* **11** (1976) 637.
14. R. W. G. WYCKOFF, 'Crystal Structures', Vol. 2 (Interscience, New York, 1951) pp. 422.
15. Y. ISHIKAWA and S. AKIMOTO, *J. Phys. Soc. Japan* **13** (1958) 1298.
16. J. J. STICKLER, S. KERN, A. WOLD and G. S. HELLER, *Phys. Rev.* **164** (1967) 765.
17. W. C. HAHN and A. MUAN, *Amer. J. Sci.* **258** (1960) 66.